K-doped CuO/ZnO with Synergistic Dual Active Centers for Highly Efficient Dimethyl Carbonate Synthesis

Han Han[1], Xue Ye[1], Jie Yao[1], Xinhua Gao[1], Jinghao Yu[1], Lisheng Guo[1], and jie Li[1]

[1]Affiliation not available

November 19, 2022

Abstract

The application of heterogeneous catalysts in dimethyl carbonate (DMC) synthesis from methanol is hindered by low activation efficiency of methanol to methoxy intermediates (CH3O*), which are the key intermediates for DMC generation. Herein, a catalyst of alkali metal K anchored on the CuO/ZnO oxide is rationally designed for offering Lewis acid-base pairs as dual active centers to improve the activation efficiency of methanol. Characterizations of CO2-TPD,XPS and DRIFTS revealed that the addition of Lewis base K observably boosted the dissociation of methanol and combined with Lewis acid CuO/ZnO oxide to stably adsorb the formed CH3O*, thus synergistically promoted the transesterification. Finally, the CuO/ZnO-9%K2O catalyst exhibited the optimal catalytic activity, achieving a high yield of 74.4% with an excellent selectivity of 98.9% for DMC at a low temperature of 90 °C. The strategy of constructing Lewis acid-base pairs provides a reference for the design of heterogeneous catalysts.

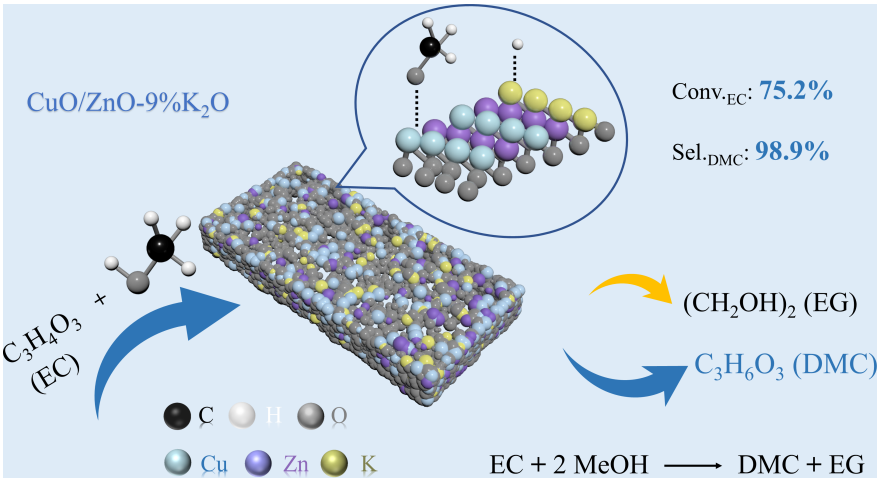

K-doped CuO/ZnO with Synergistic Dual Active Centers for Highly Efficient Dimethyl Carbonate Synthesis

Han Han[1], Xue Ye[1*], Jie Yao[2*], Xinhua Gao[3], Jinghao Yu[4], Lisheng Guo[5], and Jie Li[1*]

[1]School of Chemistry and Chemical Engineering, Yangzhou University, Yangzhou 225002, China

[2]Department of Applied Chemistry, School of Engineering, University of Toyama, Gofuku 3190, Toyama 930-8555, Japan

[3]State Key Laboratory of High-efficiency Utilization of Coal and Green Chemical Engineering, Ningxia University, Yinchuan, 750021, China

[4]Baeight Pty Ltd., Suite 6 Level 7 161 London Circuit, ACT 2601, Australia

[5]School of Chemistry and Chemical Engineering, Anhui University, Hefei 230061, China

*Correspondence

Xue Ye and Jie Li, School of Chemistry and Chemical Engineering, Yangzhou University, Yangzhou 225002, China

Email: yexue@yzu.edu.cn and jieli@yzu.edu.cn

Abstract

The application of heterogeneous catalysts in dimethyl carbonate (DMC) synthesis from methanol is hindered by low activation efficiency of methanol to methoxy intermediates (CH_3O*), which are the key intermediates for DMC generation. Herein, a catalyst of alkali metal K anchored on the CuO/ZnO oxide is rationally designed for offering Lewis acid-base pairs as dual active centers to improve the activation efficiency of methanol. Characterizations of CO_2-TPD，XPS and DRIFTS revealed that the addition of Lewis base K observably boosted the dissociation of methanol and combined with Lewis acid CuO/ZnO oxide to stably adsorb the formed CH_3O*, thus synergistically promoted the transesterification. Finally, the CuO/ZnO-9%K_2O catalyst exhibited the optimal catalytic activity, achieving a high yield of 74.4% with an excellent selectivity of 98.9% for DMC at a low temperature of 90 °C. The strategy of constructing Lewis acid-base pairs provides a reference for the design of heterogeneous catalysts.

KEYWORDS

Dimethyl carbonate, Transesterification, Copper-zinc-potassium mixed oxides, Activation and catalysis of methanol.

1. INTRODUCTION

Due to its low toxicity, easy transportation and environmental protection[1,2], dimethyl carbonate (DMC) has recently been industrially applied in various chemical syntheses, including organic intermediates and efficient solvents. In addition to replacing

phosgene via green carbonyl synthesis, the demand for DMC in emerging fields represented by electrolytes and polycarbonates is fast growing. Thus, the improvement of the DMC production process has drawn much attention. Currently, several main routes for the synthesis of DMC have been developed, including phosgenation[3], oxidative carbonylation[4–6], alcoholysis of urea[7,8], transesterification[9–12], direct methanol syntheses from CO_2[13,14], and so on. Among the routes, transesterification represents one of the main carbonate synthesis processes owing to its high atomic utilization, high yield of DMC, and mild reaction conditions.

The leading homogeneous catalyst currently used in the transesterification to synthesize DMC from ethylene carbonate (EC) and methanol is sodium methoxide[15,16]. Although the catalyst has good catalytic activity, it is sensitive to water and liable to produce strong alkaline solid waste, which causes extraordinary difficulties in product purification and catalyst recovery. In contrast, heterogeneous catalysts are easier to separate and possess higher stability, while the performance of the catalysts displays low activity due to poor mass transfer efficiency and weak methanol activation ability. Today, more literature[17–21] has reported on heterogeneous catalysts for transesterification, which generally hold high reaction temperature, long reaction time, and low DMC selectivity (Table S1). Consequently, developing an efficient heterogeneous catalyst for the transesterification synthesis of DMC under mild conditions is of great practical significance.

Wang[22] et al. found that the CH_3O* species formed by the activation of methanol with basic catalysts is the key to the synthesis of DMC. Valentina[23] et al. reported that

it was paramount for a catalyst to have a desirable dissociation and adsorption capacity of methanol. Moreover, the ability of the catalyst to stabilize the reaction intermediates also emphatically affects the performance of the catalyst. Herein, the surface of the CuO/ZnO catalyst was modified by the alkali metal K, utilizing the Lewis base property of K to facilitate the activation of methanol to form CH_3O* species, which were adsorbed and stabilized by CuO/ZnO oxide exhibiting Lewis acids. The Lewis acid-base pairs with double active centers in the catalyst can form the synergistic interaction that promotes methanol dissociation and adsorption alongside stabilizing the essential CH_3O* species. Furthermore, the experimental results suggested that changing the loading of alkali metal could effectively regulate the synergy of the double active centers to acquire the excellent-performance heterogeneous catalyst for transesterification.

2. EXPERIMENTAL

2.1. Materials

$Cu(NO_3)_2 \cdot 3H_2O$ (99.0%) and ethylene carbonate were obtained from the Shanghai Aladdin Biochemical Technology Co., Ltd., China. $Zn(NO_3)_2 \cdot 6H_2O$ (99.0%) and KNO_3 were obtained from the Sinopharm Chemical Reagent Co., Ltd. Anhydrous glucose, anhydrous ethanol and anhydrous methanol were obtained from the Shanghai Lingfeng Chemical Technology Co., Ltd. n-Butanol was obtained from the Shanghai Macklin Biochemical Co., Ltd. All the reagents and solvents were used directly without further purification.

2.2. Catalyst preparation

Firstly, carbonaceous microspheres were synthesized via the hydrothermal reaction of glucose as described elsewhere[24], and then CuO/ZnO/K_2O catalysts were prepared by the carbon microspheres-assisted template method. In a typical experiment, the copper nitrate trihydrate and zinc nitrate hexahydrate, with a molar ratio of 2.5, were made into a solution. Potassium nitrate with different proportions (molar proportions in total) was then added to the above solution. Then the solution was immersed in carbon microsphere precursor under ultrasound and aged for 2 h, followed by drying at 80 °C for 12 h. Finally, the obtained solid was calcined in an air atmosphere at 500 °C for 2 h. The prepared metal oxide product was labeled as CuO/ZnO-$x$$K_2O$, where x represented the molar percentage of potassium nitrate in the total catalyst. For comparison, CuO/ZnO/K_2O catalysts with the same composition were also prepared by coprecipitation and physical mixing and labeled as CuO/ZnO-9%K_2O (C) and CuO/ZnO-9%K_2O (PM), respectively.

2.3. Catalyst characterization

The morphology and particle size of the catalyst were studied by the field emission scanning electron microscope (SEM, s-4800, Japan), which connected with an X-ray energy dispersion spectrometer (EDS) to detect the content of various components. High-resolution transmission electron microscopy (HRTEM) was performed on the Tecnai G2 F30 S-TWIN electron microscope. The powder samples were dispersed in ethanol by ultrasound, and then transferred to a copper grid by impregnation. The X-

ray diffraction (XRD) spectrum of the catalyst was analyzed by the Bruker D8 advanced diffractometer. Under the working voltage of 40 kV and 20 mA, using monochromatic Cu Kα radiation, the angle range was 5-80 ° at room temperature, and the scanning speed was 2 °/min. Nitrogen adsorption and desorption isotherms were measured at -196 °C using the Quadrasorb EVO analyzer. The specific surface area of the catalyst was calculated by the Brunauer-Emmet-Teller (BET) method. The pore size distribution was estimated by the Barret-Joyner-Halenda (BJH) method. The basic amount and basic strength of the sample were determined by temperature-programmed desorption of CO_2 (CO_2-TPD) on the BUILDER PCA-1200 analyzer. X-ray photoelectron spectroscopy (XPS) was performed with the ESCALAB 250Xi spectrometer. Indeterminate carbon (C1s peak 284.8 eV) was used as the reference stand of binding energy. In situ Diffuse Reflectance Infrared Fourier Transform Spectroscopy (In situ DRIFTS) was analyzed with the Bruker Equinox 55 infrared spectrometer. Put the powder sample into the in-situ pool and pretreat it for 1 h under the Ar atmosphere and target temperature. Ar bubbling was used to bring methanol, and the infrared signal was collected at the same time to obtain the infrared spectrum of the methanol adsorbed intermediate.

2.4. Catalytic test

The transesterification reaction of EC and methanol was carried out in a stainless-steel autoclave equipped with magnetic stirring. At first, EC, methanol and catalyst were loaded into the reactor (the molar ratio of methanol to EC was 8 and catalyst mass accounted for 4% of the EC mass). Then the reactor was purged with nitrogen three

times, pressurized to 0.7 MPa, heated to 90 °C and stirred continuously for 5 h. After the reaction, the reactor was cooled in an ice water bath. Then, the catalyst was separated from the reaction mixture. The product mixture was quantified with GC(HF-900), equipped with the FID detector and FFAP capillary columns (60 m × 0.25 mm). The content of the product was measured by the internal standard method (n-Butanol as the internal standard). The main products were dimethyl carbonate (DMC) and ethylene glycol (EG), as well as trace products such as hydroxyethyl methyl carbonate (HEMC). EC conversion and DMC selectivity were calculated according to the following formulae:

$$\text{Conv.} = \frac{n_{EC,\,feed} - n_{EC,\,detected}}{n_{EC,\,feed}}$$

$$\text{Sel.} = \frac{n_{DMC,\,detected}}{n_{EC,\,feed} - n_{EC,\,detected}}$$

3. RESULTS AND DISCUSSION

3.1. Catalytic activity

The performance tests of CuO/ZnO-xK$_2$O catalysts and comparative catalysts were evaluated (Figure 1). In Figure 1a, the performance of the CuO/ZnO catalyst was substantially improved after adding alkali metal K. The CuO/ZnO-9%K$_2$O catalyst displayed the highest catalytic activity, and the EC conversion and DMC yield were up to 87.3% and 69.9%, respectively. In contrast, the CuO/ZnO catalyst exhibited relatively low EC conversion and DMC yield (36.1% and 19.2%, respectively). Accompanied by the change in the amount of alkali metal, the conversion of EC showed a normal distribution that first increased and then slightly decreased, thus indicating the appropriate amount of alkali metal possessed the optimal ratio. Additionally, based on

the composition of the CuO/ZnO-9%K_2O catalyst, the diversity of the catalyst obtained by different preparation methods was compared, as shown in Figure 1b, to which the catalyst prepared by the carbon microsphere-assisted template method outperformed the coprecipitation method and the physical mixing method. As for the different CuO/ZnO molar ratios (Figure 1c), their catalytic activity remained constant. Combined with Figure 1a, the synergistic interaction between the alkali metal and metal oxides is known to be affected by the preparation method, and an optimal proportion of the alkali metal exists.

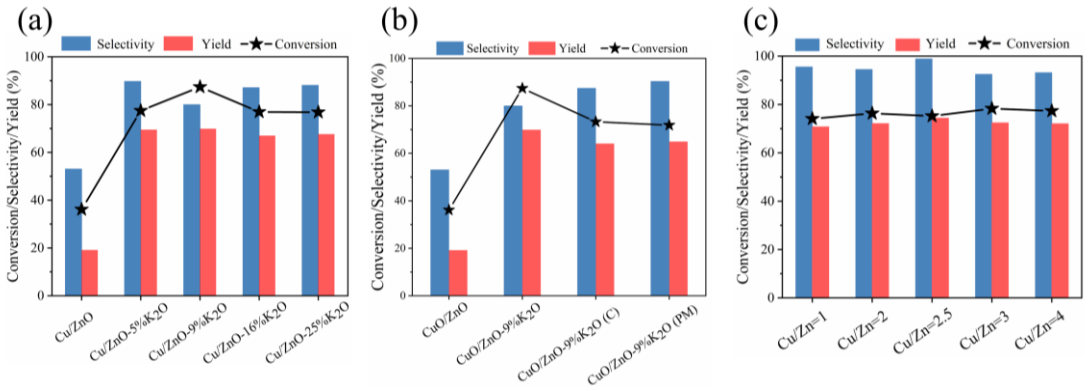

FIGURE 1 DMC yield/selectivity and EC conversion of (a) different loadings of alkali metal, (b) CuO/ZnO, CuO/ZnO-9%K_2O, CuO/ZnO-9%K_2O (C), CuO/ZnO-9%K_2O (PM), (c) different molar ratios of CuO and ZnO at 9% K_2O. Reaction conditions ((a,b) $n_{methanol}/n_{EC}$ = 8, $m_{catalyst\ dose}$ = 3 wt% of EC, T = 150 °C, t_r = 5 h. (c) $n_{methanol}/n_{EC}$ = 8, T = 90 °C, t_r = 5 h, $m_{catalyst\ dose}$ = 4 wt% of EC.)

Subsequently, the reaction parameters were further investigated, including different reaction temperatures, times, and catalyst doses (Figure S1). In Figure S1a, with the decrease in reaction temperature, the selectivity of DMC was awfully improved, indicating that a lower temperature is more favorable for converting HEMC to DMC.

At 90 °C, the optimal yield of DMC achieved 73.9%. Similarly, as the reaction time increased from 2 to 5 h, the DMC yield increased monotonically from 62.8% to 73.9%, respectively (Figure S1b). However, the yield of DMC gradually declined with time on stream, marking that the reaction had entered an equilibrium stage. The effect of catalyst dose kept pace with the above analysis of reaction parameters. The DMC selectivity and yield of the catalyst at 4 wt% were as high as 98.9% and 74.4%, respectively (Figure S1c). Compared with other heterogeneous catalysts (Table S1), we found that there were more or fewer problems such as high reaction temperature (> 130 °C) and low DMC selectivity (< 90%). This catalyst effectively improved the above problems and achieved an EC conversion of 75.2% and DMC selectivity of 98.9% at 90 °C for 5 h.

3.2. Characterization of catalyst structure

As shown in Figure 2a, the CuO/ZnO-9%K_2O catalyst exhibited a nanoparticle-like distribution. According to the HRTEM image in Figure 2b, the mean size of the CuO/ZnO-9%K_2O catalyst was about 33.75 ± 2.5nm. As was evident in Figure 2c, the lattice spacing of 0.232 nm and 0.252 nm corresponded to the (111) and (-111) crystal planes of CuO, respectively, while the lattice distance of 0.247 nm corresponded to the (101) crystal plane of ZnO. Meanwhile, the obvious particle boundary between CuO and ZnO was not found, but they contacted in the form of grain boundaries through stronger interaction, forming more discontinuous active interfaces. Although K particles were not observed, EDS elemental analysis manifested that the main metal

elements, including K, were uniformly distributed on the catalyst. Figure 2d and Figure 2e were the HRTEM images of CuO/ZnO-9%K_2O(C) and CuO/ZnO-9%K_2O(PM), respectively. The lattice spacings of 0.254 nm and 0.248 nm in Figure 2d corresponded to the CuO (-111) and ZnO (101) crystal planes, respectively. A direct comparison of Figure 2c-2e detected that the crystal particles of CuO/ZnO-9%K_2O(C) were larger than CuO/ZnO-9%K_2O. The interface between different crystals was clearer and more continuous, whereas clear particle boundaries were observed in CuO/ZnO-9%K_2O(PM), and no interaction interface was generated between CuO and ZnO. Combined with Figure 1b, the activity of the catalyst has a positive correlation with the interface of the CuO/ZnO oxide, and the catalytic performance in CuO/ZnO-9%K_2O with strong interaction and an abundant interface distinctly outstripped that of CuO/ZnO-9%K_2O (C) and CuO/ZnO-9%K_2O (PM).

As the above results reveal, the catalyst structure has a prominent impact on the catalytic performance. XRD further characterized the catalysts with different K contents, suggesting that they all displayed intact CuO and ZnO crystal phases (Figure S3). The characteristic diffraction peaks appeared at 35.5 °, 38.7 °, and 36.2 °, mainly contributing to the CuO (-111), (111) (PDF 80-1916), and ZnO (101) crystal planes (PDF 79-2205). Simultaneously, the intensity of the CuO characteristic diffraction peaks in the CuO/ZnO-*x*K_2O catalysts increased with the addition of K_2O, demonstrating that the addition of K_2O is more favorable for improving the crystallinity of CuO. Nevertheless, the characteristic diffraction peaks of K_2O were not found in the XRD spectrum, illustrating that K_2O may be in a highly dispersed state.

The decrease in the specific surface area, pore volume, and pore size of the CuO/ZnO-xK$_2$O with an increase in K$_2$O contents was displayed in Table S2, regarding the physical structure of the catalyst. Figure S4 displays the N$_2$ adsorption-desorption isotherms and pore size distributions of the CuO/ZnO-xK$_2$O catalysts. In Figure S4a, all samples showed type IV isotherms and H4 hysteresis loops, which testified that the internal structure of these catalysts was mainly mesoporous. Combined with Figure S4b, the pore size distribution of CuO/ZnO-xK$_2$O was more complicated, revealing that the mesopores were probably generated by the accumulation of catalyst nanoparticles. The XRD characterization results also demonstrated that the addition of K increased the crystallinity and crystal size of the catalyst, which in turn affected its specific surface area and pore structure.

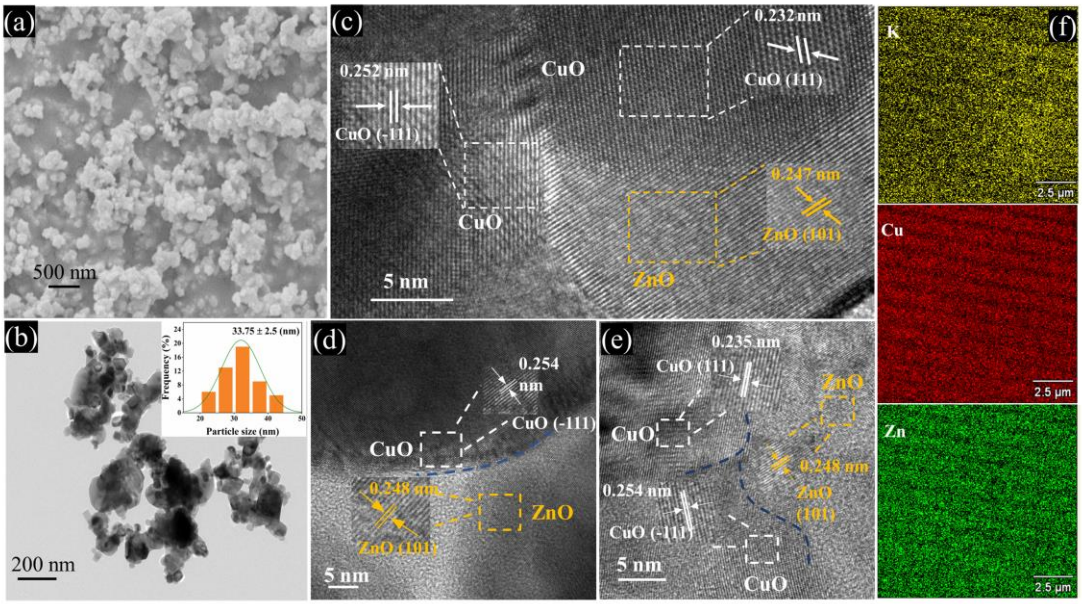

FIGURE 2 (a) SEM image of the CuO/ZnO-9%K$_2$O, (b-c) HRTEM images of the CuO/ZnO-9%K$_2$O, (d) HRTEM image of the CuO/ZnO-9%K$_2$O (C), (e) HRTEM image of the CuO/ZnO-9%K$_2$O (PM), (f) EDX element distribution of CuO/ZnO-9%K$_2$O.

Figure 1 illustrated that the addition amount of alkali metal had a significant impact on the catalyst's performance. However, there was no conspicuous difference in the structure of the catalyst accessible to the XRD and BET characterization. Therefore, CO_2-TPD technology was utilized to quantitatively analyze the basic site strength and its corresponding amounts of the CuO/ZnO-*x*K_2O catalysts. As shown in Figure 3a, an extremely weak CO_2 desorption peak was observed in the CuO/ZnO catalyst in the low-temperature range. Nevertheless, after adding K_2O, several CO_2 desorption peaks corresponded to different basic site strengths. While desorption temperatures of < 200 °C, 200-450 °C, and > 450 °C correspond to weak, medium, and strong basic sites strength, respectively[25]. As the content of K_2O increased, the total basic site amounts of the catalyst also gradually increased. However, since the content of K_2O increased to 25%, the total basic site amounts decreased instead (Figure 3b). The higher addition of alkali metal is noted to cause a decrease in alkali metal dispersion, resulting in the partial accumulation of potassium, to which this phenomenon can be attributed. In addition, the small specific surface area of CuO/ZnO-25%K_2O also decreases in the exposure of partial basic sites. Subsequently, the explicit analysis of the basic site amounts of different strengths for the series of catalysts was carried out. By comparison, the DMC yield distribution was directly proportional to the variable number of medium basic sites, with the most medium basic sites (38.0 μmol/g) in CuO/ZnO-9%K_2O, expressing that the number of medium basic sites in the catalyst plays a vital role in the catalytic performance. Furthermore, the number of strong basic sites in CuO/ZnO-

25%K_2O outclassed that of CuO/ZnO-9%K_2O, while the EC conversion was far lower than in CuO/ZnO-9%K_2O. The CuO/ZnO-16%K_2O catalyst with the strongest basic sites exhibited the lowest catalytic activity in the transesterification except for CuO/ZnO, manifesting that not all basic active site strengths have a positive effect on the catalyst.

(a)

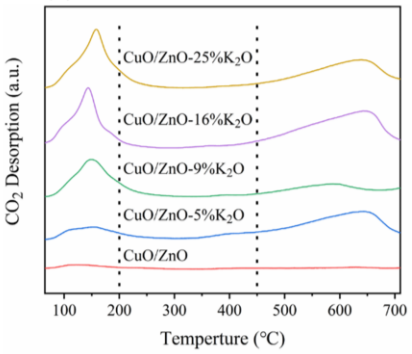

(b)

Catalyst	TPD analysis of absorbed CO_2 (μmol/g)			Total evolved CO_2 (μmol/g)
	Weak (<200 °C)	Medium (200-450 °C)	Strong (>450 °C)	
CuO/ZnO	13.5	5.3	11.6	30.4
CuO/ZnO-5% K_2O	35.1	23.7	151.3	210.1
CuO/ZnO-9% K_2O	124.3	38.0	56.2	218.5
CuO/ZnO-16% K_2O	123.2	17.6	199.2	340.0
CuO/ZnO-25% K_2O	119.5	18.8	143	281.3

CO_2-TPD analysis of CuO/ZnO-xK_2O based catalysts

FIGURE 3 (a) CO_2-TPD image of the CuO/ZnO-*x*K_2O catalysts, (b) CO_2-TPD analysis of the CuO/ZnO-*x*K_2O catalysts.

To further clarify the reasons for the effect of alkali metal addition on catalyst performance, XPS characterization provides additional insights into the electronic structure of the series of catalysts (Figure 4). In Figure 4a, the binding energies of 933.3-931.8 eV and 952.6-951.8 eV corresponded to Cu $2p_{3/2}$ and Cu $2p_{1/2}$ peaks. In addition, Cu $2p_{3/2}$ peaks at 933.1 eV belonged to Cu^{2+} species[26]. The significant jitter satellite peaks that occurred at 940.8 eV, 943.3 eV, and 961.6 eV were caused by charge transfer between the 3d orbit of transition metal and the 2p orbit of oxygen. In Figure 4b, the peaks of binding energies at 292.4-292.6 eV and 295.2-295.3 eV belonged to K $2p_{3/2}$ and K $2p_{1/2}$, respectively, which corresponded to the K^+ species. In Figure 4c, the

binding energies of 1020.7-1021.5 eV and 1043.8-1044.6 eV were ascribed to Zn $2p_{3/2}$ and Zn $2p_{1/2}$, respectively, where the distance between the two peaks (23 eV) was due to spin-orbit splitting[27]. Compared with CuO/ZnO and CuO/ZnO-9%K_2O, an incomplete reduction of Cu species took place in CuO/ZnO-9%K_2O, as evidenced by the transition from Cu^{2+} to Cu^{+} and the shift of the Cu 2p bands to lower binding energies. The phenomenon of Zn species was similar to that of Cu species, while the K species showed a rise in binding energy (manual K^{+} 295.0 eV). Based on the above results, we speculate that alkali metal K interacts with the CuO/ZnO oxide and the transfer of electrons results in the formation of the Lewis acid-base pair between them. Among them, alkali metal K can provide electrons to form the Lewis base, whereas the CuO/ZnO oxide can obtain electrons to form the Lewis acid. Through peak fitting, the change of the Cu 2p binding energy of CuO/ZnO-25%K_2O with higher alkali metal content was more significantly, which found that a large amount of Cu^{2+} was converted into Cu^{+}, and the binding energy of K species also continued to shift in a higher direction. Combined with the catalytic performance and CO_2-TPD characterization, we suggest that the activity of the catalyst is due to the synergy between the alkali metal and metal oxides, while the strong basic sites caused by adding more alkali metal led to the change in the electronic structure of the CuO/ZnO and, in turn, destroyed the synergy.

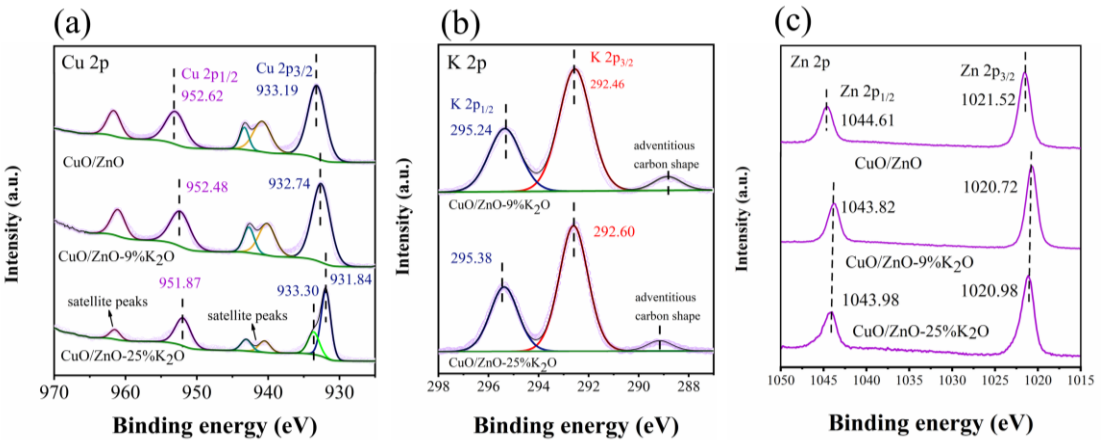

FIGURE 4 XPS spectra for (a) Cu 2p of the CuO/ZnO, CuO/ZnO-9%K_2O and CuO/ZnO-25%K_2O, (b) K 2p of the CuO/ZnO-9%K_2O and CuO/ZnO-25%K_2O, (c) Zn 2p of the CuO/ZnO, CuO/ZnO-9%K_2O and CuO/ZnO-25%K_2O.

In order to verify the synergistic effect of Lewis acid-base pairs formed between alkali metal and metal oxides and to clarify the structure-activity relationship in the catalyst, in situ diffuse reflectance infrared Fourier transform spectroscopy (DRIFTS) was utilized to characterize the degree of methanol adsorption and activation of the catalysts with different alkali metal contents (Figure 5). As shown in Figure 5a, the infrared (IR) peak at 3600-3800 cm^{-1} was assigned to the -OH stretching mode of methanol, and the IR peak at 2969 cm^{-1} was attributed to the vibration absorption peak of the methanol C-H bond[28]. Meanwhile, the IR peaks at 1460 cm^{-1} and 1450 cm^{-1} were of the bending vibration of the -CH_3 unit. The typical IR peaks attributed to CH_3O* species[29,30] (2926, 2846, 1462, 1080 cm^{-1}) were notably higher with the adsorption time passing, implying that the catalyst can adsorb and activate methanol and then generate CH_3O* active species, which is thought to be the key intermediate in transesterification. While the wide signal at ~ 1400 cm^{-1} could be ascribed to the -OH bending vibration

mode of methanol, indicating that methanol molecules are also adsorbed on the catalyst surface. Similar to Figure 5a, Figure 5b-c also show similar spectra, and the height and area of adsorption peaks were remarkably increased after the addition of alkali metal. CuO/ZnO-9%K_2O existing the strongest adsorption peaks illustrate that it possesses excellent adsorption and activation ability for methanol and thus forms more CH_3O* species. As a result, although CuO/ZnO can also activate methanol to form the key intermediate CH_3O*, the adsorption and dissociation ability of the catalyst for methanol were substantially boosted after adding alkali metal K, accompanied by the intensified ability to form active intermediates (CH_3O*). Then, the sample adsorbed methanol vapor was purged with the inert atmosphere, and the desorption results were shown in Figure 5d-f. By comparing, it was detected that the peak intensity of CuO/ZnO-25%K_2O belonging to the CH_3O* species was lower than that of CuO/ZnO-9%K_2O. Combining with CO_2-TPD and XPS characterization, we propose that the catalyst with too strong basicity affects the electronic structure of CuO/ZnO, which weakens the adsorption of CH_3O* intermediate. Based on the above analysis, it can be concluded that the activity of the catalyst comes from the alkali metal and metal oxides with an advanced synergistic dissociation-adsorption effect. The alkali metal K serves as the Lewis base active center, which affects the dissociation of methanol, while the metal oxides behave as the Lewis acids and play a key role in the stability of the active intermediate CH_3O*. Both realize the adsorption and dissociation of methanol and the further stable adsorption of the active intermediate CH_3O* through the formed Lewis acid-base pairs, which synergistically promote the transesterification. Afterwards, the

adsorption rates of a series of catalysts were further compared (Figure S5). At the beginning, the dissociation adsorption rate of the CuO/ZnO catalyst for methanol was the fastest. However, with time on stream, the different catalysts had similar adsorption rates, but the attenuation of adsorption rate is the least in CuO/ZnO-9%K_2O with the best performance. On the contrary, the adsorption rates of the other catalysts declined observably and formed an adsorption platform, which confirms that the appropriate addition of alkali metal has the optimal activity for methanol adsorption activation and affects the synergistic interaction between Lewis acid-base pairs.

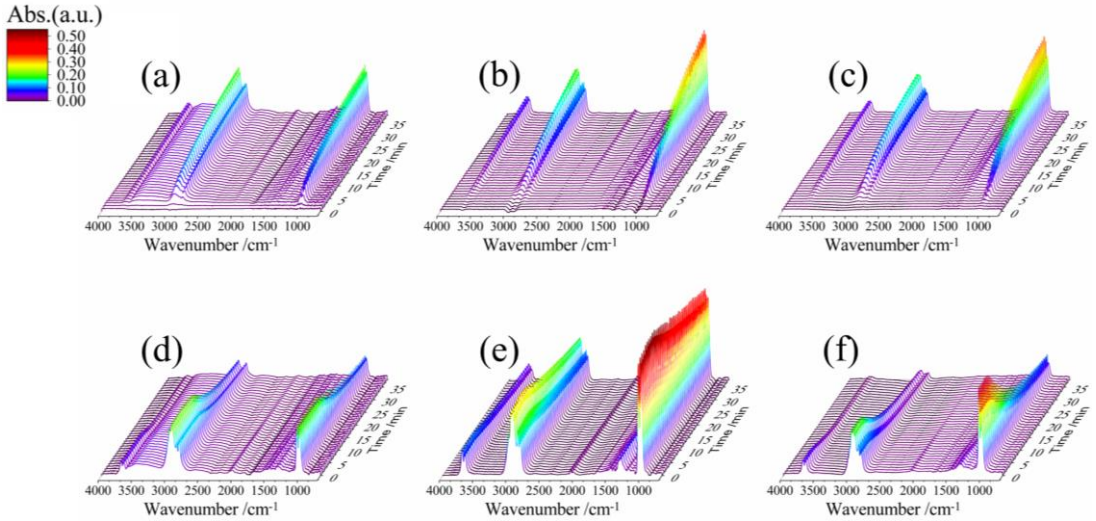

FIGURE 5 In situ FTIR spectra of methanol adsorption reaction: (a) CuO/ZnO, (b) CuO/ZnO-9%K_2O, (c) CuO/ZnO-25%K_2O and methanol desorption reaction: (d) CuO/ZnO, (e) CuO/ZnO-9%K_2O, (f) CuO/ZnO-25%K_2O.

Based on the above results and analysis of this work, we propose a possible transesterification mechanism, as shown in Scheme 1. The Lewis base was formed on the surface of the catalyst by doping with the alkali metal K and then adsorbed the

proton H^+ to boost the dissociation of methanol and generate CH_3O*. At the same time, the CuO/ZnO served as the Lewis acid adsorbed and stabilized CH_3O*. Then, CH_3O* attacked the carbonyl carbon ($C^{\delta+}$) of EC to decompose EC from cyclic ester into chain ester. Subsequently, the proton H^+ on the catalyst surface adsorbed the charged chain carbonate 1, and performed the corresponding molecular rearrangement to generate the intermediate $CH_3OCOC_2H_4OH$ (HEMC). After that, CH_3O* attacked the carbonyl carbon of HEMC again. The intermediate 2 also combined with the proton H^+ adsorbed on the catalyst surface, and finally formed dimethyl carbonate (DMC) and ethylene glycol (EG). Wang et al. proved that the second attack on the carbonyl carbon is much more arduous than the first attack. Hence, a catalyst with the strong ability to activate methanol and stabilize active intermediates (CH_3O*) is pivotal for high catalytic activity.

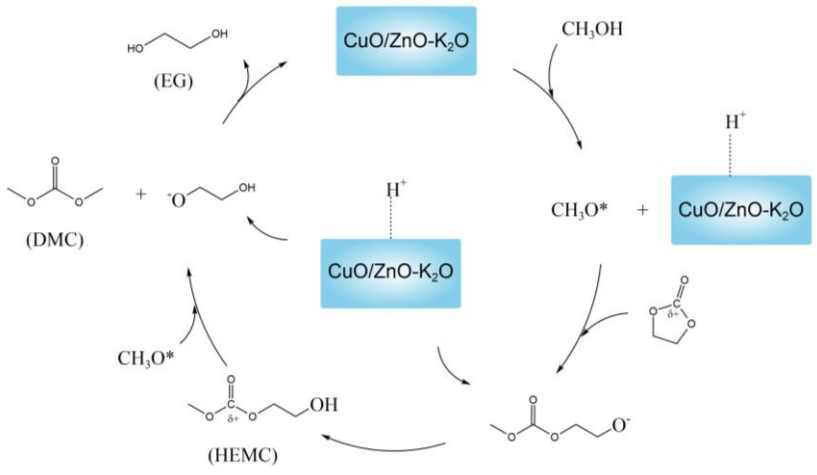

SCHEME 1 Proposed mechanism for DMC synthesis over CuO/ZnO-9%K_2O catalyst.

4. CONCLUSIONS

We report on the doping of CuO/ZnO catalysts with alkali metals K for the synthesis of

DMC via EC and methanol. The synergistic effect of the Lewis acid-base pair with double active centers composed of alkali metal K and CuO/ZnO oxide is helpful for the dissociation of methanol and the stable adsorption of the key intermediate CH_3O*, which is affected by the basicity of the catalyst. Meanwhile, adjusting the amounts of alkali metal could determine the appropriate basicity. The low alkali metal content has weaker basicity and poorer synergy, making it impossible to decompose methanol effectively. On the contrary, the higher alkali metal content causes too strong basicity, destroys the electronic structure of CuO/ZnO, weakens the stability of the catalyst on the adsorption of the key active intermediate CH_3O*, and further ruins the synergy of the catalyst. The CuO/ZnO-9%K_2O catalyst exhibited the best basicity and intermediate stabilization ability, as well as the best DMC selectivity (98.9%) and DMC yield (74.4%). Our work provides new insights and references for the design and synthesis of heterogeneous catalysis to complete the synthesis of DMC and highlights the potential for industrial application with reasonable design ideas and high catalytic performance.

CONFLICT OF INTEREST

The authors declare no potential conflict of interest.

ACKNOWLEDGMENTS

This work was supported by the National Natural Science Foundation of China (22002135 and 22208283); Natural Science Foundation of the Jiangsu Higher

Education Institutions of China (20KJB480004); Foundation of State Key Laboratory of High-efficiency Utilization of Coal and Green Chemical Engineering (No. 2022-K49); and Yangzhou City Lvyangjinfeng Project of China.

REFERENCES

1. Quadrelli EA, Centi G, Duplan JL, Perathoner S. Carbon dioxide recycling: Emerging large-scale technologies with industrial potential. *ChemSusChem*. 2011;4(9):1194-1215. doi:10.1002/cssc.201100473
2. Ding X, Dong X, Kuang D, Wang S, Zhao X, Wang Y. Highly efficient catalyst $PdCl_2$-$CuCl_2$-KOAc/AC@Al_2O_3 for gas-phase oxidative carbonylation of methanol to dimethyl carbonate: Preparation and reaction mechanism. *Chem Eng J*. 2014;240:221-227. doi:10.1016/j.cej.2013.11.079
3. Delledonne D, Rivetti F, Romano U. Developments in the production and application of dimethylcarbonate. *Appl Catal A Gen*. 2001;221(1-2):241-251. doi:10.1016/S0926-860X(01)00796-7
4. Yamamoto Y, Matsuzaki T, Tanaka S, et al. Catalysis and characterization of Pd/NaY for dimethyl carbonate synthesis from methyl nitrite and CO. *J Chem Soc - Faraday Trans*. 1997;93(20):3721-3727. doi:10.1039/a702015e
5. Wang C, Xu N, Liu TT, et al. Mechanical pressure-mediated Pd active sites formation in NaY zeolite catalysts for indirect oxidative carbonylation of methanol to dimethyl carbonate. *J Catal*. 2021;396:269-280. doi:10.1016/j.jcat.2021.03.009
6. Shi R, Wang J, Zhao J, et al. Cu nanoparticles encapsulated with hollow carbon spheres for methanol oxidative carbonylation: Tuning of the catalytic properties by particle size control. *Appl Surf Sci*. 2018;459(79):707-715. doi:10.1016/j.apsusc.2018.08.032
7. Wang M, Zhao N, Wei W, Sun Y. Synthesis of dimethyl carbonate from urea and methanol over metal oxides. *Stud Surf Sci Catal*. 2004;153:197-200. doi:10.1016/s0167-2991(04)80247-7
8. Keller N, Rebmann G, Keller V. Catalysts, mechanisms and industrial processes for the dimethylcarbonate synthesis. *J Mol Catal A Chem*. 2010;317(1-2):1-18. doi:10.1016/j.molcata.2009.10.027
9. Stoica G, Abelló S, Pérez-Ramírez J. Na-dawsonite derived aluminates for DMC production by transesterification of ethylene carbonate. *Appl Catal A Gen*. 2009;365(2):252-260. doi:10.1016/j.apcata.2009.06.022
10. Wei Q, Hu J, Zhang H, Wang G, Yang X. Efficient Synthesis of Dimethyl Carbonate via Transesterification from Ethylene Carbonate with Methanol Using $KAlO_2$/γ-Al_2O_3 Heterogeneous Catalyst. *ChemistrySelect*. 2020;5(26):7826-7834. doi:10.1002/slct.202001641
11. Gan YL, Hu XQ, Wen LZ, Xu J, Xue B. Metal-free synthesis of dimethyl

carbonate: Via transesterification of ethylene carbonate catalyzed by graphitic carbon nitride materials. *New J Chem*. 2020;44(8):3215-3223. doi:10.1039/c9nj04530a

12. Zheng H, Hong Y, Xu J, Xue B, Li YX. Transesterification of ethylene carbonate to dimethyl carbonate catalyzed by CeO_2 materials with various morphologies. *Catal Commun*. 2018;106(October 2017):6-10. doi:10.1016/j.catcom.2017.12.007
13. Bian J, Xiao M, Wang SJ, Lu YX, Meng YZ. Carbon nanotubes supported Cu-Ni bimetallic catalysts and their properties for the direct synthesis of dimethyl carbonate from methanol and carbon dioxide. *Appl Surf Sci*. 2009;255(16):7188-7196. doi:10.1016/j.apsusc.2009.03.057
14. Abate S, Barbera K, Giglio E, et al. Synthesis, Characterization, and Activity Pattern of Ni-Al Hydrotalcite Catalysts in CO_2 Methanation. *Ind Eng Chem Res*. 2016;55(30):8299-8308. doi:10.1021/acs.iecr.6b01581
15. Fang YJ, Xiao W De. Experimental and modeling studies on a homogeneous reactive distillation system for dimethyl carbonate synthesis by transesterification. *Sep Purif Technol*. 2004;34(1-3):255-263. doi:10.1016/S1383-5866(03)00198-9
16. Keller T, Holtbruegge J, Niesbach A, Górak A. Transesterification of dimethyl carbonate with ethanol to form ethyl methyl carbonate and diethyl carbonate: A comprehensive study on chemical equilibrium and reaction kinetics. *Ind Eng Chem Res*. 2011;50(19):11073-11086. doi:10.1021/ie2014982
17. Wang H, Wang M, Liu S, Zhao N, Wei W, Sun Y. Influence of preparation methods on the structure and performance of CaO-ZrO_2 catalyst for the synthesis of dimethyl carbonate via transesterification. *J Mol Catal A Chem*. 2006;258(1-2):308-312. doi:10.1016/j.molcata.2006.05.050
18. Watanabe Y, Tatsumi T. Hydrotalcite-type materials as catalysts for the synthesis of dimethyl carbonate from ethylene carbonate and methanol. *Microporous Mesoporous Mater*. 1998;22(1-3):399-407. doi:10.1016/S1387-1811(98)00099-7
19. Dhuri SM, Mahajani V V. Studies in transesterification of ethylene carbonate to dimethyl carbonate over Amberlyst A-21 catalyst. *J Chem Technol Biotechnol*. 2006;81(1):62-69. doi:10.1002/jctb.1358
20. Pyrlik A, Hoelderich WF, Müller K, Arlt W, Strautmann J, Kruse D. Dimethyl carbonate via transesterification of propylene carbonate with methanol over ion exchange resins. *Appl Catal B Environ*. 2012;125:486-491. doi:10.1016/j.apcatb.2011.09.033
21. Xu J, Long KZ, Chen T, Xue B, Li YX, Cao Y. Mesostructured graphitic carbon nitride as a new base catalyst for the efficient synthesis of dimethyl carbonate by transesterification. *Catal Sci Technol*. 2013;3(12):3192-3199. doi:10.1039/c3cy00517h
22. Wang JQ, Sun J, Cheng WG, et al. Synthesis of dimethyl carbonate catalyzed by carboxylic functionalized imidazolium salt via transesterification reaction. *Catal Sci Technol*. 2012;2(3):600-605. doi:10.1039/c1cy00342a

23. Crocellà V, Tabanelli T, Vitillo JG, et al. A multi-technique approach to disclose the reaction mechanism of dimethyl carbonate synthesis over amino-modified SBA-15 catalysts. *Appl Catal B Environ*. 2017;211:323-336. doi:10.1016/j.apcatb.2017.04.013
24. Sun X, Liu J, Li Y. Use of carbonaceous polysaccharide microspheres as templates for fabricating metal oxide hollow spheres. *Chem - A Eur J*. 2006;12(7):2039-2047. doi:10.1002/chem.200500660
25. Kumar P, Kaur R, Verma S, Srivastava VC, Mishra IM. The preparation and efficacy of SrO/CeO_2 catalysts for the production of dimethyl carbonate by transesterification of ethylene carbonate. *Fuel*. 2018;220(January):706-716. doi:10.1016/j.fuel.2018.01.137
26. Hu X, Qin W, Guan Q, Li W. The Synergistic Effect of CuZnCeOx in Controlling the Formation of Methanol and CO from CO_2 Hydrogenation. *ChemCatChem*. 2018;10(19):4438-4449. doi:10.1002/cctc.201800668
27. Zhang Y, Ji Y, Li J, Liu H, Zhong Z, Su F. Hierarchical zinc-copper oxide hollow microspheres as active Rochow reaction catalysts: The formation and effect of charge transferable interfaces. *J Catal*. 2017;348:233-245. doi:10.1016/j.jcat.2017.02.030
28. Wang Y, Wang K, Zhang B, et al. Direct Conversion of CO_2 to Ethanol Boosted by Intimacy-Sensitive Multifunctional Catalysts. *ACS Catal*. 2021;11(18):11742-11753. doi:10.1021/acscatal.1c01504
29. Cui WG, Li YT, Yu L, Zhang H, Hu TL. Zeolite-Encapsulated Ultrasmall Cu/ZnOx Nanoparticles for the Hydrogenation of CO_2 to Methanol. *ACS Appl Mater Interfaces*. 2021;13(16):18693-18703. doi:10.1021/acsami.1c00432
30. Qi T, Zhao Y, Chen S, et al. Bimetallic metal organic framework-templated synthesis of a Cu-ZnO/Al_2O_3 catalyst with superior methanol selectivity for CO_2 hydrogenation. *Mol Catal*. 2021;514(July):111870. doi:10.1016/j.mcat.2021.111870